URSI AP-RASC 2019, New Delhi, India; 09 - 15 March 2019

ScaRaB onboard Megha Tropiques (MT) observations of seasonal mean diurnal variations of cloud radiative forcing (CRF) at top-of-atmosphere over tropics and the impact of El Niño periods (November 2014-February 2016) on CRF

Ashok Kumar Gupta[(1)], K. Rajeev[(1)], and Manoj Kumar Mishra[(1)]
(1) Space Physics Laboratory, VSSC, Thiruvananthapuram, 695022

Abstract

The ScaRaB payload onboard Megha-Tropiques (MT) satellite has been making observations of radiative fluxes at the top of the atmosphere (TOA) for different local time (LT) of the day. This provides a unique opportunity to investigate the diurnal variation of the regional instantaneous cloud radiative Forcing (CRF) at TOA. Using direct observations of radiative fluxes from ScaRaB, seasonal mean diurnal variations of CRF at TOA are investigated during July 2012-Decemeber 2016. Such observations are essential to investigate and quantify the regional differences in the longwave CRF (LWCRF) diurnal cycle and daytime variations of shortwave CRF (SWCRF) over deep convective regions and subsidence zones of the Hadley and Walker circulation cells. One of the most remarkable features observed is the significantly large diurnal variation of LWCRF over deep convective regions, with distinctly different phases over the continents and open oceans. Results show that the magnitude of the diurnal variation of LWCRF is largest over the continental deep convective regions of Brazil and Africa, where the peak-to-trough amplitude of the diurnal cycle of LWCRF is in the range of 20 to 30 Wm^{-2}, which is about 30-45% of their diurnal mean values. Peak-to-trough amplitude of the diurnal cycle of LWCRF over the oceanic regions are mostly in the range of $\sim$15 to 25Wm^{-2} which are about 20 to 35% of the diurnal mean values of LWCRF over these regions. The least diurnal variation of LWCRF over the ITCZ generally occurs over the eastern Pacific (peak-to-trough amplitude $<$15 Wm^{-2}). The diurnal maxima of LWCRF over the continental regions occur during 15-21 LT while the minima occur at $\sim$03-09 LT. Over the deep convective regions of open oceans, the diurnal cycle of LWCRF attains broad maximum during 21-06 LT while the minimum occurs at $\sim$09-12 LT. Further, this study indicates that the magnitudes of shortwave CRF (SWCRF) are largest around $\sim$12-15 LT, mainly due to the largest incoming solar flux and phase of the diurnal variation of cloud development. Though significant shift in the location of deep convection occurs during El Nino periods (which also introduces corresponding shift in the spatial variations of LWCRF and SWCRF), zonal variations of the average net CRF (NCRF) during the El Nino and normal periods are remarkably similar during all seasons.

1 Introduction

Diurnal cycle is a fundamental mode of variability in most of the meteorological parameters, which is primarily forced by daily variations in solar insolation. Diurnal variation of cloud development and their radiative impact play a pivotal role in modulating the diurnal cycle of energy budget of the surface and atmosphere [e.g., Ramanathan et al., 1989 and references therein]. Phases of the diurnal cycles of cloud development and their radiative impact depend on their generation mechanisms. In particular, phase of the diurnal cycle of convection is an important parameter in determining the cloud radiative forcing [e.g., Nowicki and Merchant, 2004]. In general, development of convective clouds peaks in the afternoon over continental regions, while the organized convection over oceanic regions generally peak during late night or early morning. Similarly, marine stratocumulus cloud amount starts increasing from just before the local sunset and attains its peak before dawn, while the lesser cloud amount is often reached in the afternoon owing to the maximum rate of cloud break up occurring around noon (following the warming of the surface by incoming solar radiation).

Radiative effects of clouds have been investigated extensively in the past [e.g., Ramanathan et al., 1989; Roca et al., 2005; Sathiyamorthy et al., 2013; Taylor, 2012; Thampi and Roca, 2014; Saud et al., 2016]. Most of these studies were carrried out using satellite based observations over the last four decades. However, these observations are made at fixed local time of the day (e.g., 10:30 AM/PM, 01:30 AM/PM) and hence do not cover the diurnal cycle. CERES flown onboard the low-inclination TRMM satellite provided direct observations of the TOA radiances at different local times of the day during the satellites precession cycle. These observations could be carried out only for limited period and were used for estimating the diurnal variations of aerosol and cloud radiative effects [e.g., Rajeev and Ramanathan, 2001; Christopher et al., 2003]. Another methodology used to derive the diurnal variation of cloud radiative forcing (CRF) is by utilizing the broadband radiative fluxes estimated from geostationary satellite observations of the narrow band visible and IR observations [e.g., Nowicki and Merchant, 2004], which have lesser accuracy compared to the direct observations of broadband radiances

at TOA.

Direct observations of the seasonal mean diurnal variations of cloud radiative forcing can be estimated from the observations carried out using ScaRaB/3 payload flown onboard the low-inclination Megha-Tropiques satellite, utilizing its capability to observe all regions at all local time bins during its 51-days precession cycle. The main advantage of this technique is that the diurnal variation of CRF can be estimated directly over the entire tropics from the MT-ScaRaB/3 observations compared to the diurnally interpolated values from CERES (e.g., CERES-Terra synoptic data) or limiting the direct estimates to fixed local times of the day. Major limitations of MT-ScaRaB/3 estimates of CRF are: (i) these estimates can be carried out only on a seasonal mean basis as the diurnal cycle for all tropical locations are covered only during the 51-days orbit precession cycle of MT, and (ii) the frequency of observations at a given local time during any season is fewer than that from the sun-synchronous CERES which make observations every day at two fixed local times.

Main objective of the present study is to estimate the multi-year (2012-2016) seasonal mean diurnal variations (averaged at 3-hourly intervals) of longwave CRF (LWCRF) and daytime variations of shortwave CRF (SWCRF) over the tropics and investigate their temporal and seasonal variations and the net cloud radiative impact. The uncertainties arising from any bias in the observations are minimised by using the seasonal mean cloud-free reference values of the SW and LW radiative fluxes at $1^o \times 1^o$ geographical grids estimated at different local times from the MT-ScaRaB/3 observation itself in the estimation of SWCRF and LWCRF at TOA. Overall uncertainty of LWCRF is less than 7% while that of SWCRF is $\sim$17%. The results obtained from this study are summarized below.

2 Data and Method

Megha-Tropiques has an orbital inclination of 19.98° and an orbital period of 101.93 minutes. During its 51-day precession cycle, MT-ScaRaB/3 observations cover all local times at all geographical locations, which are repeated after the 51-days cycle. This unique nature of MT-ScaRaB/3 observations is utilized here to derive the diurnal variation of SWCRF and LWCRF over the tropics. MT-ScaRaB/3 measures radiances at four independent spectral bands: (i) Channel-1- visible band (0.55-0.65 μm), (i) Channel-2 - shortwave band (0.2-4.0 μm), (iii) Channel-3 - total spectral band (0.2 to 100 μm), (iv) Channel-4 - IR window band (10.5-12.5 μm). Radiances measured using channels-1 and -4 are used for scene identification and cloud detection. The longwave radiances are estimated by subtracting the radiances observed in channel-2 (shortwave band) from channel-3 (total spectral band) after giving weightage for the spectral response functions. The radiances are calibrated using onboard calibration system [Viollier and Raberanto, 2010]. The observations are carried out using cross track scanning mode, with each scan line having 51 pixels (swath of 2200 km). Pixel resolution of MT-ScaRaB/3 at nadir is 40 km. Resolution of the edge pixel in the scan line is about 90 km. In the present analysis 4 edge pixels on either side of each scan line are not used due to their poor spatial resolutions. MT-ScaRaB/3 can make observations of radiances up to $\pm 30^\circ$ latitude over tropics, because of the 2200 km wide swath.

The level-2 MT-ScaRaB/3 data comprising of the instantaneous TOA fluxes in the shortwave and longwave spectral bands covering the entire tropics during the period of July 2012-February 2016 are used in the present study. Cloud radiative forcing is defined as the difference between the mean radiative fluxes under all-sky condition minus those for the clear-sky condition [Ramanathan et al., 1989; Roca et al., 2005].. Thus, the CRF at TOA can be determined from the following relations:

$$SWCRF = -(SWF_{obs} - SWF_{clearsky}) \quad (1)$$

$$LWCRF = -(LWF_{obs} - LWF_{clearsky}) \quad (2)$$

$$NCRF = SWCRF + LWCRF \quad (3)$$

In the above equations, $SWF_{clearsky}$ and $LWF_{clearsky}$ are the cloud-free SW and LW fluxes for each geographical region of $1^\circ \times 1^\circ$ at fixed local time intervals during a season. Estimates of CRF are carried out from each pixel and are averaged at 3 hourly local time (LT) intervals during each season (following an equivalent day analysis) over the entire tropics with a geographical grid of 1°x1° (latitude $\times$ longitude). Utilization of the cloud-free reference fluxes for each season and year are determined from the MT-ScaRaB/3 observations, which remove the effects of any biases in the observed radiances while deriving the SWCRF and LWCRF.

3 Results

3.1 Zonal variations of LWCRF: diurnal amplitude and phase

Zonal variation of the diurnal cycles of LWCRF over the equatorial region (averaged between 10°N and 10°S) during different seasons are depicted in Figure 1. This is obtained by subtracting the seasonal mean (diurnal average) value of LWCRF from the individual 3-hourly values for each longitude bin of 2° grid size. Figure 1 shows that, during all seasons over the equatorial region, largest amplitude of the diurnal variation occurs over continental regions (central American region: $\sim$85°W to $\sim$40°W; central African region: $\sim$10°W to $\sim$40°E). The peak-to-trough variation of the diurnal cycle over the central American region is in the range of 15 to 25 Wm^{-2}. Over the central African region, the peak-to-trough diurnal amplitude varies between 10 and 30 Wm^{-2}. Over the African region, Figure 1 shows less diurnal amplitude at west of 10°E compared to its east. This is mainly because, between 10°S and 10°N, the surface type is a combination of land and ocean in the former region,

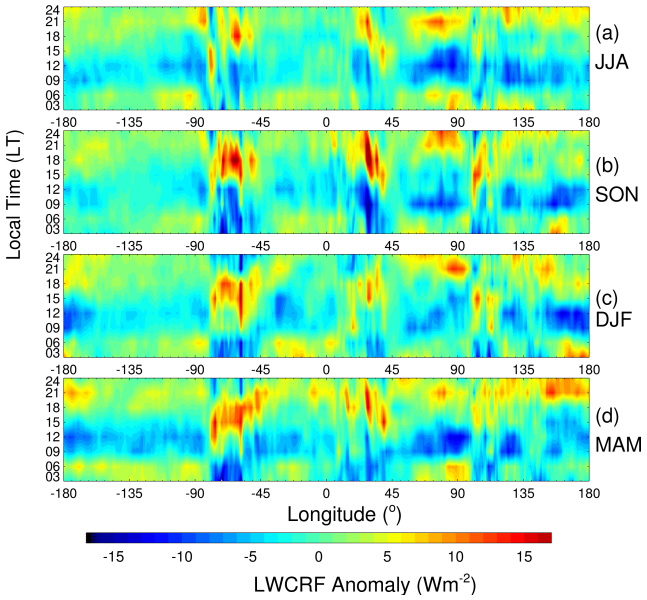

Figure 1. Zonal variation of the diurnal cycles of LWCRF over the equatorial region (averaged between 10°N and 10°S) during different seasons (averaged during 2012-2016). The mean values of LWCRF (averaged within 10°N and 10°S) at each longitude are removed.

while it is completely continental at east of 10°E. Over the central African region, largest diurnal amplitude of LWCRF is observed between ∼24°E and ∼34°E during all seasons. Over both the central American and central African regions, the diurnal cycle is most prominent during northern autumn (September-November), which is followed by spring. The diurnal amplitude is generally weaker during summer over the central American region. Phases of the diurnal variations over the central American and central African regions are somewhat similar, with the minimum occurring at 03-06 LT and maximum occurring at 15-21 LT. This is primarily due to the convection triggered by large land surface heating during the afternoon.

Phase of the diurnal cycle of LWCRF is somewhat similar over all the open oceanic regions and is distinctly different from the continental regions. Over open oceans, diurnal peak of LWCRF is rather broad and occurs during 21-06 LT, while the diurnal minimum occurs during 09-12 LT. The tendency for diurnal maximum to occur during ∼21-00 LT is more over most of the oceanic regions. Largest diurnal amplitude of LWCRF over oceanic regions (peak-to-trough amplitude of ∼20 Wm^{-2}) is observed over the Indian Ocean (during all seasons except northern spring) and the central Pacific (during northern spring), and while the lowest diurnal amplitude is observed over the eastern Pacific and the Atlantic (peak-to-trough variation of 8 to 15 Wm^{-2}). The diurnal cycle over the Indonesian archipelagos has a mixed phase, though its amplitude is quite significant (15 to 20 Wm^{-2}). The minimum LWCRF occurs mostly at 09-12 LT (similar to the continents and open oceans), while the diurnal peak occurs between 15 LT (especially over the western parts) and 00 LT (over the eastern parts). This might be because of the dominating effect of landmass (bigger islands) over the western parts and that of the open ocean (tiny island chain) over the eastern parts.

3.2 Zonal variations of seasonal mean longwave-, shortwave- and net- CRF over the equatorial region

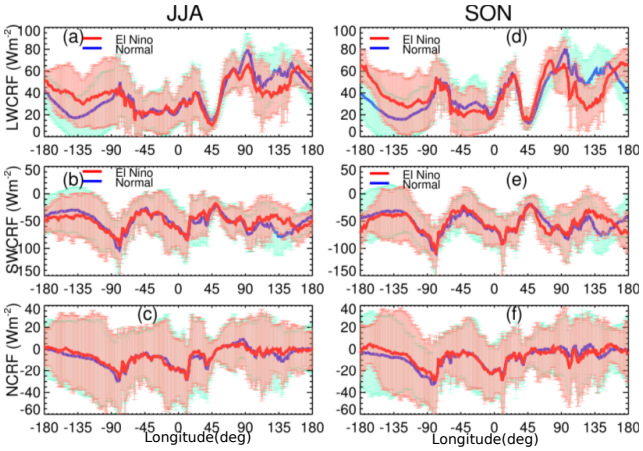

Figure 2. Zonal variations of the seasonal mean diurnally averaged LWCRF, SWCRF and NCRF averaged over the equatorial region (10°S to 10°N) during the four seasons for the normal (July 2012-October 2014) and El Niño periods (November 2014-February 2016). The vertical bars indicate the standard deviations.

The Walker circulation introduces significant longitude variations of convection and cloudiness. This will cause corresponding variations in cloud radiative forcing and their spatial gradients. The longitude variations of cloudiness and CRF would be different during El Niño periods. The El Niño conditions prevailed during November 2014 to May 2016 (Oceanic Nino Index, ONI > 0.5), with moderate and strong phases of El Niño during May 2015 to April 2016 (ONI in the range of 1 to 2.6). In the present study, CRF during the El Niño period is averaged separately to investigate the effect of El Niño on CRF. Zonal variations of the seasonal mean (diurnally averaged) LWCRF, SWCRF and NCRF averaged over the equatorial region (10°S to 10°N) for the four seasons of normal period (mean for 2012-2014) and El Niño period (November 2014 to February 2016) are shown in Figure 2. Major features observed in Figure 2 are given below.

Substantial zonal gradients are observed in SWCRF, LWCRF and NCRF in all seasons during the normal and El Niño periods. These include the large-scale gradients between the ascending and descending limbs of the Walker cells as well as the rapid variations having smaller spatial scales. The latter includes drastic spatial variations in LWCRF, SWCRF and NCRF associated with convection across the coastal regions like those appearing over the west coast of Brazilian sector (at ∼80°W) almost throughout the

year and the west coast of equatorial Africa (at $\sim$10°E) during northern summer and autumn. In contrast, systematic and large-scale spatial gradients of LWCRF, SWCRF and NCRF occurs between the east and the west equatorial Indian Ocean, associated with the Walker cell. Similar features are also seen over the African and American longitudes. In general, magnitude of the NCRF is quite small ($<$10 Wm^{-2}) over the deep convective oceanic regions, while significant negative NCRF values are observed over the continental deep convective regions. This is primarily because of the phase of the diurnal variation of convection, which shows its peak during afternoon (and hence considerable magnitude of SWCRF) over the continents compared to the oceanic regions where the peak occurs during night (and hence have smaller magnitude of SWCRF).

During the normal period, the western Pacific witnesses strong deep convective zone with high magnitudes of SWCRF and LWCRF, while the central and the eastern Pacific have relatively smaller magnitudes. In contrast, during the El Niño period, magnitudes of LWCRF and SWCRF decreases significantly ($\sim$20 to $\sim$30 Wm^{-2}) over the western Pacific while their values increase considerably (by $\sim$20 to $\sim$40 Wm^{-2}) over the central and eastern Pacific. This is associated with the eastward movement of the convective zone from the western Pacific to the central and the eastern Pacific during the El Niño periods. Though significant spatial variations occur in the LWCRF and SWCRF between the normal and El Niño periods, zonal variations of the net CRF during the El Niño and normal periods are similar during seasons. This is because the decrease in the diurnal mean LWCRF is compensated by decrease in the diurnal mean SWCRF by an equal magnitude.

4 Discussion and Summary

This paper presents the direct observations of diurnal cycle of LWCRF and daytime variations of SWCRF and their temporal seasonal variations. Such observations are essential to investigate and quantify the regional differences in the LWCRF diurnal cycle and daytime variations of shortwave CRF over deep convective regions and subsidence zones of the Hadley and Walker circulation cells. Magnitude of the diurnal variation is largest over the continental deep convective regions of Brazil and Africa, where the peak-to-trough amplitude of the diurnal cycle of LWCRF is mostly in the range of 20 to 30 Wm^{-2},which is about 30-45% of their diurnal mean values. The diurnal maxima of LWCRF over these continental regions occur during 15-21 LT while the minima occur at $\sim$03-09 LT. Over the deep convective regions of open oceans, the diurnal cycle of LWCRF attains broad maximum during 21-06 LT while the minimum occurs at $\sim$09-12 LT. To better understand the radiative impact of different cloud types requires radiation budget data with daily or better time resolution. Analysis using high time resolution data will help to understand the causes of the variability observed in the radiative impact of clouds, and the extent to which it is associated with changes in cloud fraction.

5 Acknowledgements

Megha-Tropiques-ScaRaB observed Fluxes data were obtained from MOSDAC data system (www.mosdac.gov.in/) maintained by ISRO. Ashok Kumar Gupta was supported by ISRO Research Fellowship

References

[1] S. A. Christopher, J. Wang, Q. Ji, and S.-C. Tsay (2003), Estimation of diurnal shortwave dust aerosol radiative forcing during pride, J. Geophys. Res., 108 (D19), doi:1029/2002JD002787.

[2] S. M. Nowicki, and C. J. Merchant (2004), Observations of diurnal and spatial variability of radiative forcing by equatorial deep convective clouds, J. Geophys. Res., 109(D11), doi:10.1029/2003JD004176.

[3] V. Ramanathan , R. D. Cess, E. F. Harrison, P. Minnis, B. R. Barkstrom, E. Ahmad, and D. Hartmann, "Cloud-radiative forcing and climate: results from the Earth radiation budget experiment," *Science* **243** (4887), 57-63, doi:10.1126/science.243.4887.57.

[4] R. Roca, S. Louvet, L. Picon, and M. Desbois (2005), A study of convective systems, water vapor and top of the atmosphere cloud radiative forcing over the Indian Ocean using INSAT-1B and ERBE data, Meteorol. Atmos. Phys., 90 (1-2), 49-65.

[5] K. Rajeev, and V. Ramanathan (2001), Direct observations of clear-sky aerosol radiative forcing from space during the Indian Ocean Experiment, J. Geophys. Res., 106 (D15), 17,221, doi:10.1029/2000JD900723.

[6] V. Sathiyamoorthy, B. P. Shukla, R. Sikhakolli, S. Chaurasia, B. Simon, B. Gohil, and P. Pal, "Top of atmosphere flux from the Megha-Tropiques ScaRaB", *Curr. Sci.*, pp. 1656-1661, 2013.

[7] T. Saud, S. Dey, S. Das, and S. Dutta, A satellite-based 13-year climatology of net cloud radiative forcing over the Indian monsoon region, *Atmos. Res.* **182**, 76-86, 2016 doi:10.1016/j.atmosres.2016.07.017.

[8] P. C. Taylor (2012), Tropical outgoing longwave radiation and longwave cloud forcing diurnal cycles from CERES, J. Atmos. Sci., 69 (12), 3652-3669.

[9] B. Thampi, and R. Roca (2014), Investigation of negative cloud radiative forcing over the Indian subcontinent and adjacent oceans during the summer monsoon season, Atmos. Chem. Phys., 14 (13), 6739-6758.

[10] M. Viollier, and P. Raberanto (2010), Radiometric and spectral characteristics of the ScaRaB-3 instrument on Megha-Tropiques: comparisons with ERBE, CERES, and GERB, J. Atmos. Oceanic Technol., 27 (3), 428-442, doi: 10.1175/2009JTECHA1307.1.